



Hybrid catalysts with enhanced C₃H₆ resistance for NH₃-SCR of NO_x

Qi Zhao^a, Bingbing Chen^a, Zhifeng Bai^a, Limei Yu^a, Mark Crocker^{b,*}, Chuan Shi^{a,*}

^a State Key Laboratory of Fine Chemicals, School of Chemistry, Dalian University of Technology, Dalian, 116024, China

^b Center for Applied Energy Research, University of Kentucky, Lexington, KY, 40511, USA



ARTICLE INFO

Keywords:
NH₃-SCR
Propene poisoning resistance
Fe-Beta
MnO_x/CeO₂
DRIFTS

ABSTRACT

Utilization of Fe-Beta for NH₃-SCR of NO_x in diesel engine applications is severely limited by hydrocarbon poisoning. In this work, a series of hybrid catalysts are prepared by mechanical mixing of zeolites and oxides, and their activity for the selective catalytic reduction of NO_x with NH₃ is investigated in the presence of propene. Results have shown that a catalyst prepared by mixing Fe-Beta and MnO_x/CeO₂ in a mass ratio of 1:1 exhibits high SCR activity. NO_x conversion in the temperature range 200–400 °C has exceeded 90% at a GHSV of 80,000 h⁻¹, with low selectivity to N₂O. By the combined DRIFTS and MS measurements, the function of MnO_x/CeO₂ in the hybrid catalysts is discussed. This hybrid catalyst is able to convert C₃H₆ to intermediates containing C=O and COO functionalities, thereby decreasing carbon deposition on the zeolite and reduce the competitive adsorption between C₃H₆ and NO_x. Moreover, these intermediates react with NO_x at lower temperatures than do the carbonaceous deposits on Fe-Beta, enhancing the NO_x reduction activity.

1. Introduction

Selective catalytic reduction (SCR) by urea or ammonia is one of the most commonly applied technologies for the abatement of nitrogen oxides (NO_x) in the presence of excess oxygen [1]. Metal exchanged zeolites, which in recent years have attracted much attention in the field of NH₃-SCR, are commercial catalysts used for automobile exhaust purification, normally exhibiting excellent performance over a wide temperature range (200–650 °C) [1–4].

Fe-containing zeolites, especially for Fe-Beta catalysts, present better high temperature activities compared with commercial Cu-SSZ-13 catalysts, with the former typically displaying better resistance to sulfur poisoning [1,5,6]. By employing Al-rich Beta zeolites as a substrate for Fe, low temperature activity (≤ 200 °C) can be maximized, enabling the application of Fe-Beta catalysts in NH₃-SCR of NO_x [1,7,8]. However, owing to the fact that Beta zeolites possess relatively large pores and cages than SSZ-13 (pore diameters of approximately 6.5 Å and 3.8 Å, respectively), catalyst activity is inhibited in the presence of hydrocarbons which possess small kinetic diameters (such as propene, 4.5 Å) due to coke deposition in the zeolite channels [3,9]. Besides the effect of intrinsic pore structure, zeolites with strong acidity are more susceptible towards deactivation by hydrocarbons, because hydrocarbons can adsorb on the acid sites to ultimately form coke deposits [10,11]. In recent years, the poisoning of SCR catalysts by hydrocarbons and possible methods to reduce the consequences have been

studied by a number of researchers [10,12–17]. Luo et al. [18] found that dodecane decreased Cu-Beta's NH₃-SCR activity at 150 °C due to its physical adsorption in the zeolite pores that blocked access to active sites. Ma et al. [10] designed a novel fully formulated Fe-BEA monolith catalyst coating modified with MOR, the deactivation of Fe-BEA due to propene poisoning being clearly reduced.

On the other hand, manganese - based oxide catalysts not only exhibit particularly high activity for low temperature NH₃-SCR, but also act as superior oxidation catalysts for a variety of volatile organic compounds (VOCs) combustion reactions [19–21]. Inspired by the dual properties of manganese - based catalysts, we propose a novel approach to reduce the negative effects of C₃H₆ on Fe-Beta catalysts by mechanical mixing of MnO_x/CeO₂ oxide with Fe-Beta zeolite. The reason for choosing CeO₂ as co-component is that ceria is potentially advantageous for NH₃-SCR, e.g. broadening the SCR temperature window, enhancing high temperature activity and improving N₂ selectivity and resistance to poisoning by SO₂ [19,22–24]. Hypothetically, the oxide can oxidize C₃H₆ and consequently reduce its inhibiting effect on the NH₃-SCR reaction. As we shown in this paper, hybrid catalysts consisting of MnO_x/CeO₂ mixed with Fe-Beta (with optimized mass ratios) do indeed greatly improve SCR activity in the presence of C₃H₆, albeit the mechanism behind the enhancement is not exactly as anticipated. Based on in situ DRIFTS measurements, combined with MS studies, the roles of MnO_x/CeO₂ and Fe-Beta zeolite in NH₃-SCR in the presence of C₃H₆ were clarified in the present study.

* Corresponding authors.

E-mail addresses: mark.crocker@uky.edu (M. Crocker), chuanshi@dlut.edu.cn (C. Shi).

2. Experimental

2.1. Catalyst preparation

The zeolite support was organotemplate-free Na-Beta zeolite with a Si/Al ratio of 9 which was obtained from BASF, Germany. The synthesis of this zeolite has been reported elsewhere [25]. Before use, Na-Beta underwent a conventional ion-exchange process to bring it into the NH_4^+ form. Using NH_4 -Beta as precursor, a 2 wt% iron-containing zeolite catalyst was prepared by incipient wetness impregnation (IWI) with a solution of ferrocene in toluene at room temperature, followed by calcination at 500 °C in air for 4 h using a heating rate of 4 °C min⁻¹. This material is henceforth referred to as Fe-Beta.

The $\text{MnO}_x/\text{CeO}_2$ catalyst was prepared by a deposition – precipitation method. Typically, an appropriate amount of aqueous Mn (NO_3)₂ solution was mixed with CeO_2 powder (Rare - Chem Hi - Tech Co., Ltd., China), and then an aqueous solution of Na_2CO_3 was added dropwise under continuous stirring until the pH reached 8.5 – 9.0. The precipitate was aged for 1 h at room temperature, after which the mixture was filtered and washed with deionized water. The resulting solid was dried at 110 °C and then calcined in air at 400 °C for 4 h. The target Mn concentration was determined to be 50 wt%. Pure manganese oxide was prepared by the same procedure used for $\text{MnO}_x/\text{CeO}_2$, except for the addition of the CeO_2 support.

The hybrid catalysts were prepared by mechanically grinding different amounts of Fe-Beta and oxides, followed by calcining the mixtures at 500 °C in air. The hybrid catalysts were denoted as follows: FM = Fe-Beta + MnO_x (with a mass ratio of 3:1); FC = Fe-Beta + CeO_2 (with a mass ratio of 3:1); FMC1 to FMC3 = Fe-Beta + $\text{MnO}_x/\text{CeO}_2$ for which the mass ratio of zeolite and oxide was varied from 1:1 to 3:1. All samples were pressed, crushed, and sieved to 40–60 mesh to obtain suitable particles for the experiments.

2.2. Catalyst characterization

X-ray diffraction (XRD) measurements were carried out on an X-ray diffractometer (Rigaku D/Max 2400) with $\text{Cu K}\alpha$ radiation ($\lambda = 1.5404 \text{ \AA}$) in a 2θ range of 5 – 90° at a scanning speed of 0.02° s⁻¹.

Hydrogen temperature programmed reduction (H_2 -TPR) experiments were performed on a Micromeritics AutoChem II 2920 chemisorption analyzer. A sample of ~50 mg was placed in a U-shape quartz reactor. The catalysts were first pretreated at 300 °C in Ar for 1 h, then cooled down to the room temperature. Subsequently, a mixture of 5% H_2/Ar (100 ml min⁻¹) was fed to the reactor and the temperature was linearly increased to 600 °C at a rate of 10 °C min⁻¹.

X-ray photoelectron spectroscopic (XPS) measurements were conducted by ESCALAB250 Thermo VG spectroscopy using an Al $\text{K}\alpha$ source operating at 15 kV and 10 mA. C 1 s at 284.6 eV was used as an internal binding energy standard to correct for charging effects.

2.3. Techniques

In situ DRIFTS measurements were performed on a Bruker Tensor 27 spectrometer equipped with MCT detector. The catalyst was first pretreated in He at 300 °C for 1 h, then cooled down to the test temperature, and a background spectrum was recorded at each measured temperature under flowing of He. NH_3 , $\text{C}_3\text{H}_6 + \text{O}_2$, $\text{NO} + \text{C}_3\text{H}_6 + \text{O}_2$ and $\text{NO} + \text{O}_2$ adsorption were performed by flowing the appropriate gas for 0.5 h and then purging with He for another 15 min at the same temperature. After the adsorption and purging steps, the He flow was switched to other flowing gases to achieve a so-called transient surface reaction, e.g., $\text{NH}_3 \rightarrow \text{NO} + \text{O}_2$, or $\text{NH}_3 \rightarrow \text{NO} + \text{O}_2 + \text{C}_3\text{H}_6$. DRIFT spectra were then recorded periodically as a function of reaction time, 60 scans being accumulated in each case at a resolution of 4 cm⁻¹.

Identical transient procedures were carried out using an online mass spectrometer (MS, Omini-star, GSD-300) to detect the effluent gases

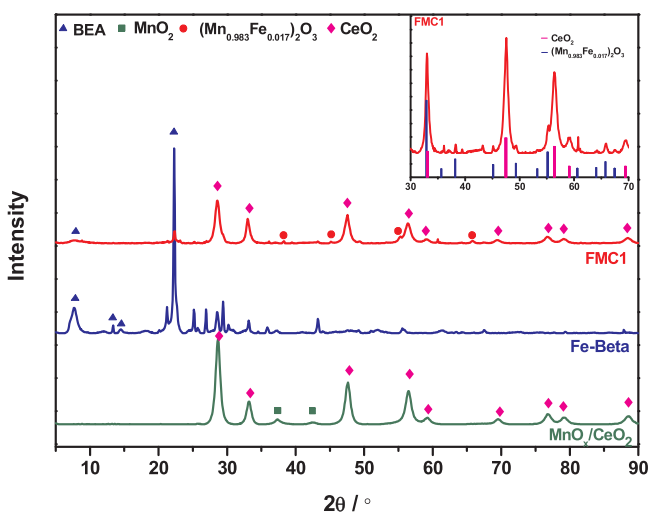


Fig. 1. XRD patterns of the indicated catalysts.

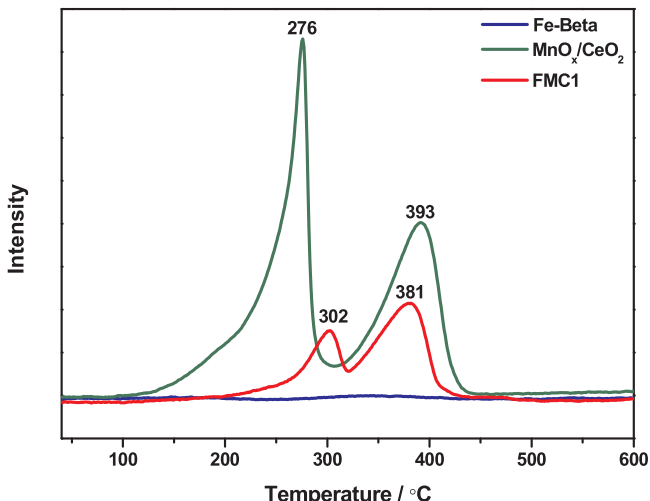


Fig. 2. H_2 -TPR profiles of different catalysts. Conditions: 5% H_2/Ar ; flow rate: 100 ml/min; ramp rate: 10 °C/min.

during the surface reaction. The masses characteristic of NO (30), NH_3 (17), O_2 (32), N_2 (28, 14), H_2O (18), N_2O (29, 44, 45), CO (14, 28), CO_2 (22, 44, 45), C_3H_6 (41, 42), NO_2 (46) were recorded. Competitive adsorption experiments were conducted by using 50 mg catalyst in a quartz reactor. The adsorption was performed by passing a gas mixture containing 500 ppm NO and 5% O_2 , or 500 ppm NO, 500 ppm C_3H_6 , 5% O_2 and Ar as balance gas through the sample bed at RT for 1 h with the total flow rate of 200 ml min⁻¹. After the adsorption, the system was purged with Ar until no NO_x or C_3H_6 were detected in the effluent. TPD measurements were carried out up to 700 °C with a heating rate of 10 °C min⁻¹ in flowing of Ar.

2.4. Catalytic activity measurements

The NH_3 -SCR activity measurements were conducted with 180 mg of the sample using a fixed-bed quartz microreactor (i.d. 6 mm). Before each experiment, the catalyst was first pretreated in N_2 for 1 h at 500 °C, and then cooled down to desired temperature. Then the catalyst was exposed to a reactant gas mixture containing 500 ppm NO, 500 ppm NH_3 , 500 ppm C_3H_6 (when used), 10% O_2 , 10% CO_2 , 5% H_2O and balanced N_2 , and the total flow rate was 400 ml min⁻¹. NO, NO_2 , NO_x (= NO + NO_2), NH_3 and N_2O concentrations were monitored continuously using a NO_x analyzer (Ecophysics, Switzerland) and an NH_3

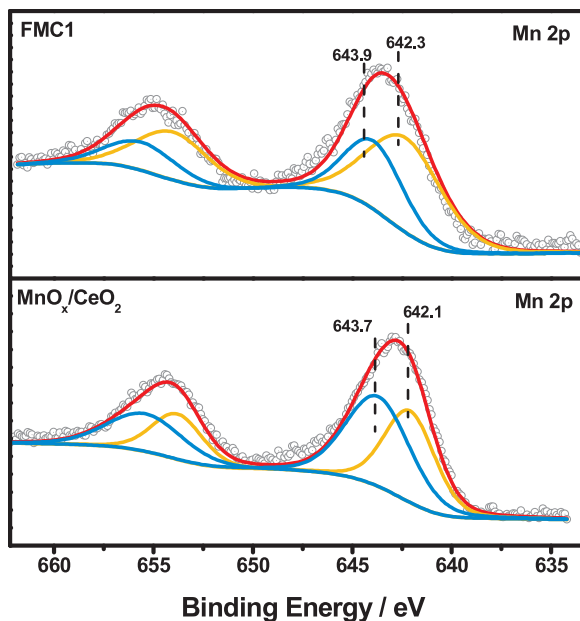


Fig. 3. XPS spectra of $\text{MnO}_x/\text{CeO}_2$ and FMC1 in the Mn 2p region.

N_2O analyzer (Sick Maihak, Germany), respectively. All data were obtained when the SCR reaction reached a steady state at each temperature. C_3H_6 oxidation activity was monitored by an online non-dispersive infrared analyzer (SICK-MAIHAK-S710, Germany) which recorded the concentration of CO and CO_2 . A Cu-Mn/Al₂O₃ catalyst was used to completely oxidize C_3H_6 into CO_x at 500 °C [26,27], the amount of CO_x generated being used to quantify the C_3H_6 concentration.

3. Results and discussion

3.1. Catalyst structural characterization

In order to ascertain whether any structural transformations occurred during mechanical mixing of the catalyst components, sample FMC1 was subjected to analysis. For reference purposes, Fe-Beta and $\text{MnO}_x/\text{CeO}_2$ were also analyzed.

XRD patterns for the samples are displayed in Fig. 1. The characteristic reflections of the BEA framework [25] and CeO_2 (JCPDS no. 43-1002) can both be observed for the FMC1 sample. Notably, the X-ray

peak intensity of CeO_2 is relatively higher than that of MnO_x . As indicated in the slow scan XRD pattern from 26 to 31° (Fig. S1), a shift of the diffraction peak to higher Bragg angles can be observed for $\text{MnO}_x/\text{CeO}_2$ with respect to CeO_2 [28]. The lattice constant calculated for CeO_2 is 5.410 Å, while that for $\text{MnO}_x/\text{CeO}_2$ is 5.404 Å. Hence, the observed decrease in the lattice constant is evidence of the formation of a Mn-Ce-O solid solution [29,30]. However, due to the high fraction of MnO_x in $\text{MnO}_x/\text{CeO}_2$, a discrete manganese oxide phase is present on the catalyst surface, giving rise to MnO_x diffraction peaks. After mechanical mixing of Fe-Beta with $\text{MnO}_x/\text{CeO}_2$, the reflections for Fe-Beta have become extremely weak, the CeO_2 reflections being much stronger compared to Fe-Beta. This might be related to coating of the zeolite by $\text{MnO}_x/\text{CeO}_2$ particles, as shown by TEM images (Fig. S2), leading to the lower intensity of zeolite diffraction lines. Similar results have been reported in the literature [17]. In addition, a new phase corresponding to $(\text{Mn}_{0.983}\text{Fe}_{0.017})_2\text{O}_3$ (JCPDS no. 24-0507) is detected, as clearly shown in the inset figure. This suggests that chemical interactions occur between Fe-Beta and $\text{MnO}_x/\text{CeO}_2$ upon calcination.

Fig. 2 shows H_2 -TPR profiles recorded for FMC1, Fe-Beta and $\text{MnO}_x/\text{CeO}_2$. There are two major H_2 consumption peaks at 302 °C and 381 °C for the FMC1 sample. By comparison with the profile of $\text{MnO}_x/\text{CeO}_2$, the peak at 381 °C can be assigned to the reduction of Mn^{3+} to Mn^{2+} [21,31]. Relative to $\text{MnO}_x/\text{CeO}_2$, the first peak is weaker and shifted to higher temperature, and can be ascribed to the formation of the $(\text{Mn}_{0.983}\text{Fe}_{0.017})_2\text{O}_3$ phase which leads to a change in the chemical states of Mn. This has been further confirmed by XPS results shown in Fig. 3.

Two kinds of Mn species are present in XPS profiles (Fig. 3). The peak at $\text{BE} = 642.1\text{--}642.3$ eV can be assigned to Mn^{3+} [32,33], while that at $\text{BE} = 643.7\text{--}643.9$ eV is assigned to Mn^{4+} [33,34]. Deconvolution of the peaks enables the distribution of Mn species to be estimated. The ratio of $\text{Mn}^{3+}/(\text{Mn}^{3+} + \text{Mn}^{4+})$ is 63.5% for FMC1, which is higher than that of $\text{MnO}_x/\text{CeO}_2$ (44.6%), indicating that FMC1 is enriched with Mn^{3+} .

3.2. Catalytic activity

NO_x conversion and N_2O yield as a function of reaction temperature over the Fe-based catalysts are shown in Fig. 4. NH_3 -SCR activity below 300 °C is severely depressed by the presence of C_3H_6 in the feed gas over Fe-Beta catalyst (Fig. 4(A)), as compared to the experiment with no hydrocarbon present (shown as a grey dotted line in Fig. 4(A)). The activity of the hybrid catalysts, corresponding to CeO_2 , MnO_x , and $\text{MnO}_x/\text{CeO}_2$ mixed with Fe-Beta zeolite at a fixed weight ratio of 1:3, is

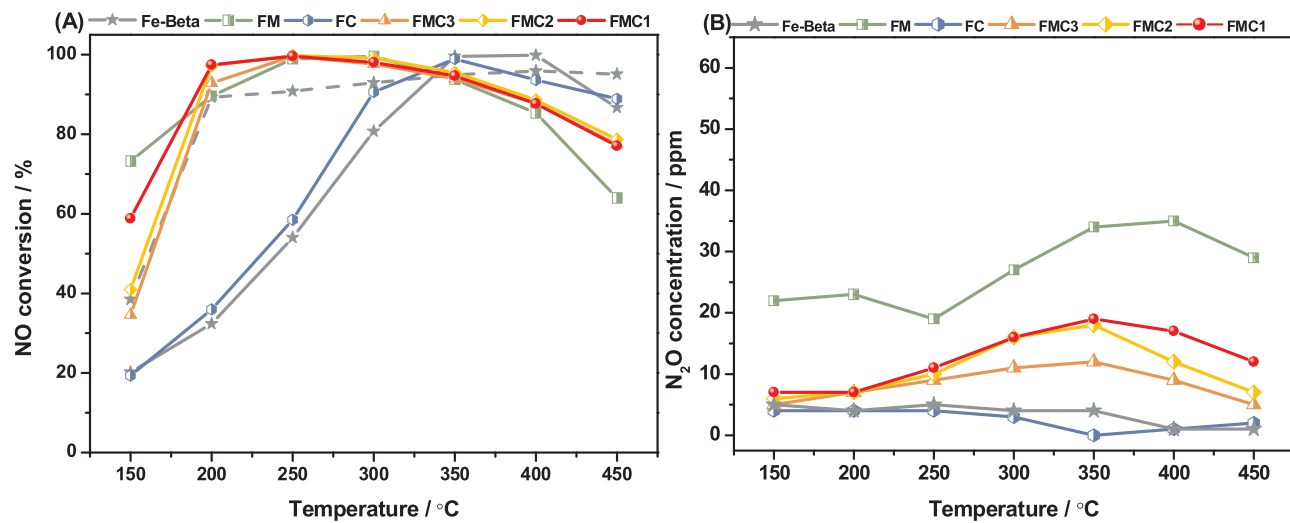


Fig. 4. NH_3 -SCR performance in the presence of C_3H_6 (A) and N_2O yield (B) of the indicated catalysts, the activity of Fe-Beta in the absence of C_3H_6 being shown as the grey dotted line in the figure. Conditions: 500 ppm NO, 500 ppm NH_3 , 500 ppm C_3H_6 , 10% O_2 , 10% CO_2 , 5% H_2O and N_2 balance, GHSV = 80,000 h^{-1} .

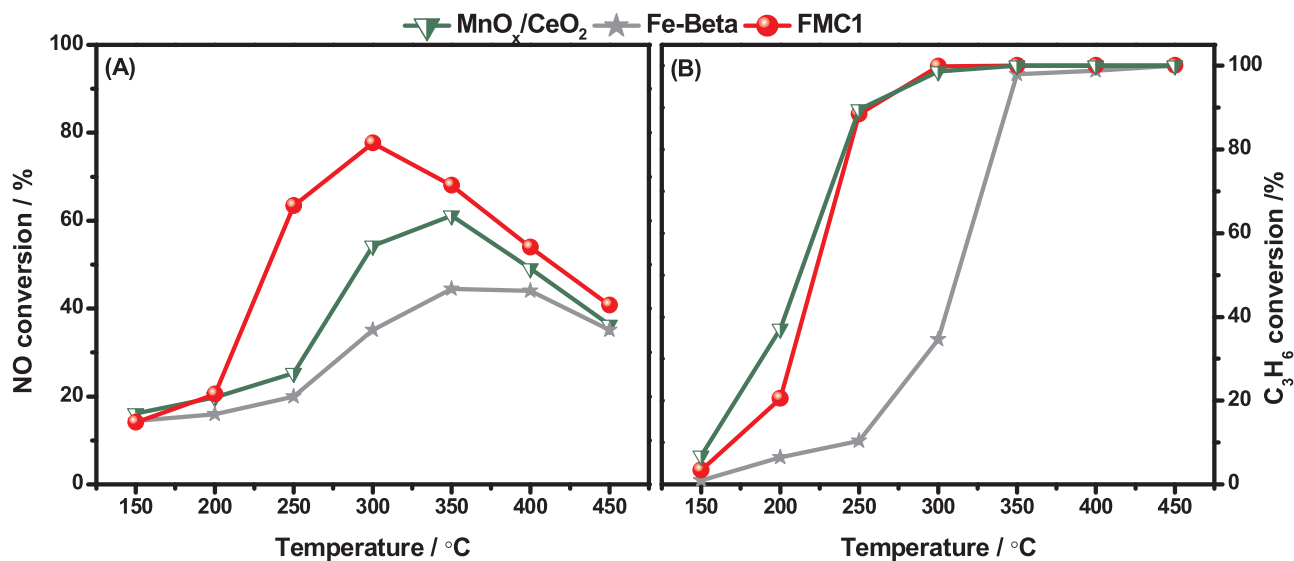


Fig. 5. C₃H₆-SCR (A) and C₃H₆ oxidation activity (B) of the indicated catalysts. Conditions: (A) 500 ppm NO, 500 ppm C₃H₆, 10% O₂, 10% CO₂, 5% H₂O and N₂ balance, (B) 500 ppm C₃H₆, 10% O₂ and N₂ balance, GHSV = 80,000 h⁻¹.

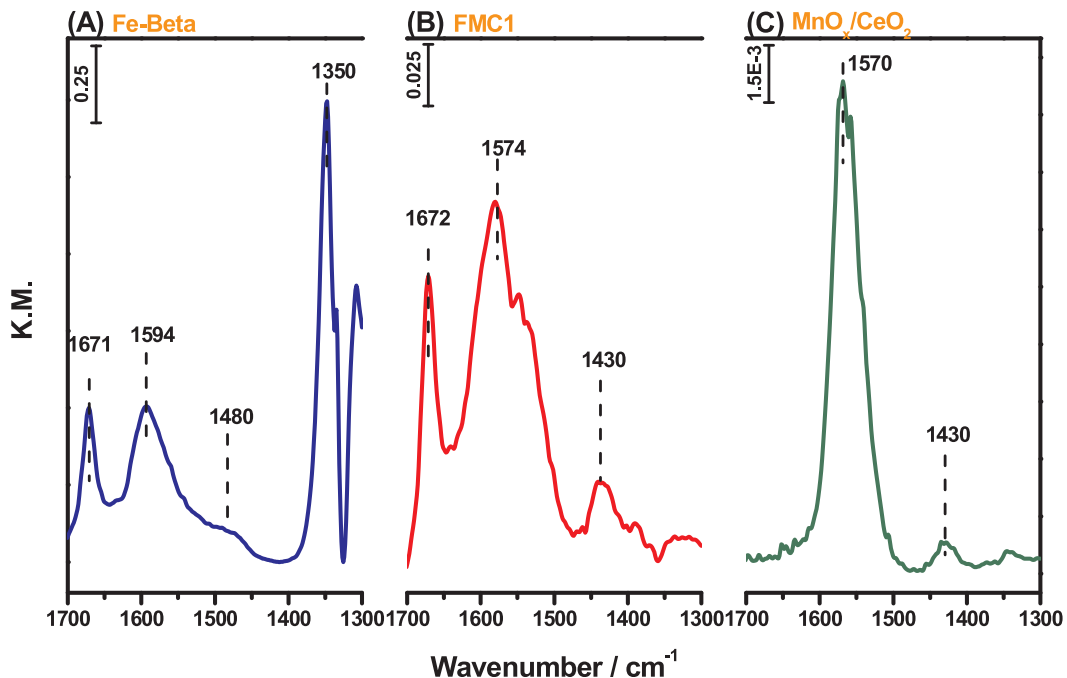


Fig. 6. IR spectra of (A) Fe-Beta, (B) FMC1 and (C) MnO_x/CeO₂ after exposure to 500 ppm C₃H₆/10% O₂/He at 150 °C for 30 min.

also evaluated. Although addition of CeO₂ to Fe-Beta zeolite has little influence on the activity, mixing Fe-Beta with MnO_x improved the low temperature activity. NO_x conversion over FM and FMC3 has reached 73.3% and 34.6% at 150 °C respectively. Upon further increase of the temperature, NO_x conversion has decreased gradually, especially over the FM catalyst, which should be due to the occurrence of a side reaction of NH₃ oxidation catalyzed by MnO_x. Meanwhile, significant N₂O formation is observed over FM compared with FC and FMC3. The yield of N₂O (shown in Fig. 4(B)) has presented two basic trends in the present study: N₂O has been observed to increase with temperature as well as with the fraction of MnO_x in the catalyst, indicating that N₂O has been formed from the NH₃ oxidation reaction, which is preferentially catalyzed by MnO_x and favored at higher temperature [35]. In addition, it is known that MnO_x/CeO₂ possesses better SO₂ resistance than MnO_x itself and thus FMC3 exhibited better SO₂ resistance than

FM, as shown in Fig. S3 [36]. Given these trends, MnO_x/CeO₂, as opposed to MnO_x, has been employed for this study, the ratio of Fe-Beta to MnO_x/CeO₂ being optimized. Upon decrease of the weight ratio of the zeolite to mixed oxide from 3:1 to 1:1, the low temperature activity has been greatly enhanced, NO conversions of 58.8% and 96.9% being obtained at 150 °C and 200 °C respectively. Moreover, better high temperature activity has also been obtained for FMC1 compared with other hybrid catalysts. These results give clear evidence that the mixture of MnO_x/CeO₂ oxide with Fe-Beta zeolite provides simple and effective approach for maintaining the superior performance of Fe-Beta zeolite in NH₃-SCR in the presence of C₃H₆.

The catalytic performance of Fe-Beta, MnO_x/CeO₂ and FMC1 in C₃H₆-SCR of NO_x and C₃H₆ oxidation has also been evaluated in an attempt to ascertain whether MnO_x/CeO₂ catalyzed the C₃H₆-SCR of NO_x directly or whether it was responsible for oxidation of C₃H₆ to CO_x,

Table 1
Assignments of FTIR bands observed during related reaction process.

Species	Wavenumber (cm ⁻¹)	
	References	This work
$\nu_s(\text{COO})$	1430–1457 [37,38]	1430
$\nu_{\text{as}}(\text{COO})$	1540–1580 [37,38]	1570–1574
$\nu(\text{C}=\text{C})$ in $\pi\text{-C}_3\text{H}_5$	1490–1510 [39,40]	1480
$\nu(\text{C}=\text{C})$ in allylic	1372–1379 [40,41]	1350
$\nu(\text{C}=\text{C})$ in polyene	1605–1590 [39,40,42]	1594
$\nu(\text{C}=\text{O})$	1668, 1684–1725 [43,44,45]	1670–1695
NH_4^+	1465–1470 [46,47,48]	1474–1485
Coordinated NH_3	1602–1610 [33,46,47,49]	1600–1620
$\nu_s(\text{NO}_2)$	1320 [50]	1313–1334
$\nu(\text{NO}_3^-)$	1293, 1320, 1550–1684 [38,43,46,47,50,51]	1280, 1430–1447, 1530, 1570, 1583, 1602, 1629
$\nu_{\text{as}}(\text{NO}_2)$	1420–1500 [50]	1480
$\nu(\text{N}_2\text{O}_3)$	1684 [47]	1684
$\nu(\text{NO}_2)$	1675 [46]	1668
Gaseous NO	1878 [46,47]	1870–1880
$\nu(\text{CH}_3)$	2890–2924 [40,42,44]	2926

thereby eliminating the negative effects of C_3H_6 on Fe-Beta. In the case of C_3H_6 -SCR, as shown in Fig. 5(A), NO_x conversion over all three of the catalysts is quite poor at temperatures below 250 °C. For example, NO_x conversion is 20.5% over FMC1 at 200 °C, much lower than the 97.4% NO_x conversion observed in NH_3 -SCR. This suggests that the improvement in low temperature activity induced by the mixed oxide is not a consequence of the C_3H_6 -SCR reaction. For C_3H_6 oxidation, as shown in Fig. 5(B), the conversions obtained below 200 °C are also quite poor for all of the catalysts. The C_3H_6 conversion over FMC1 catalyst is below 20% at 200 °C, which indicates that the enhanced activity resulting from addition of the mixed oxide (especially at temperatures below 200 °C) can not be ascribed to the direct combustion of C_3H_6 into CO_x ($x = 1$ or 2). In addition, it is noteworthy that a 50% yield of CO has been obtained over Fe-Beta, in comparison to CO yields of less than 5% over the mixed oxide and hybrid catalysts due to their higher activity for oxidation as shown in Fig. S4. The fact that CO is generated as a secondary pollutant over Fe-Beta when C_3H_6 is presented, highlights the benefits of applying the catalyst mixture in the NH_3 -SCR reaction.

3.3. Co-adsorption of $\text{C}_3\text{H}_6 + \text{O}_2$

The function of the mixed oxide in the NH_3 -SCR reaction has been examined by coupling in situ DRIFTS for the detection of surface intermediates and MS for the analysis of gas phase species. Fig. 6 shows IR spectra of Fe-Beta, $\text{MnO}_x/\text{CeO}_2$ and FMC1 after exposure to 500 ppm $\text{C}_3\text{H}_6 + 10\% \text{O}_2$ for 30 min at 150 °C followed by purging in He for another 15 min. The detailed descriptions of IR bands are displayed in Table 1. For the Fe-Beta sample, four bands appeared, which are assigned to $\nu(\text{C}=\text{O})$ (1671 cm⁻¹), $\nu(\text{C}=\text{C})$ in a polyene (1594 cm⁻¹), $\nu(\text{C}=\text{C})$ in $\pi\text{-C}_3\text{H}_5$ (1480 cm⁻¹) and $\nu(\text{C}=\text{C})$ in an allylic group (1350 cm⁻¹). These results indicate that C_3H_6 is adsorbed on the Fe-Beta surface and that adsorbed C_3H_6 is apt to polymerize as evidenced by the presence of polyene, $\pi\text{-C}_3\text{H}_5$ and allylic groups. The presence of such polymerized species can be expected to result in blocking of the zeolite pores. In the case of FMC1, the main peaks observed belong to $\nu(\text{C}=\text{O})$ (1672 cm⁻¹), $\nu_s(\text{COO})$ (1574 cm⁻¹) and $\nu_{\text{as}}(\text{COO})$ (1430 cm⁻¹), suggesting that C_3H_6 is partially oxidized on the catalyst to form adsorbed oxygenates. After saturation with $\text{C}_3\text{H}_6 + \text{O}_2$ for 30 min over the $\text{MnO}_x/\text{CeO}_2$ oxide, only two peaks can be observed which can be assigned to carboxyl species. From these results, it is clear that FMC1 and $\text{MnO}_x/\text{CeO}_2$ are more active than Fe-Beta for C_3H_6 oxidation, preventing the polymerization of C_3H_6 on the Fe-Beta zeolite.

3.4. Competitive adsorption of NO_x with C_3H_6

In situ DRIFTS studies of $\text{NO} + \text{O}_2$ adsorption on Fe-Beta, FMC1 and $\text{MnO}_x/\text{CeO}_2$ have been carried out, both with and without C_3H_6 , the results being shown in Fig. 7. Upon exposure of Fe-Beta, peaks at 1684, 1602, 1583 and 1447 cm⁻¹ are observed. These bands are attributed to the asymmetric stretching frequency of gaseous NO_2 , overlapped with bands due to bridged nitrate (1602 cm⁻¹), bidentate nitrate and monodentate nitrate (1583 cm⁻¹), monodentate nitrate (1447 cm⁻¹) and adsorbed N_2O_3 (1684 cm⁻¹). When C_3H_6 is added to the feed, new bands at 1676 and 1594 cm⁻¹ have appeared which are assigned to $\nu(\text{C}=\text{O})$ and $\nu(\text{C}=\text{C})$ bands of polyene, respectively. A weak band at 1480 cm⁻¹ is also observed, which can be ascribed to $\nu_{\text{as}}(\text{NO}_2)$. It can be seen that the formation of adsorbed NO_x species is sharply depressed when C_3H_6 is present, which may be due to occupation of adsorption

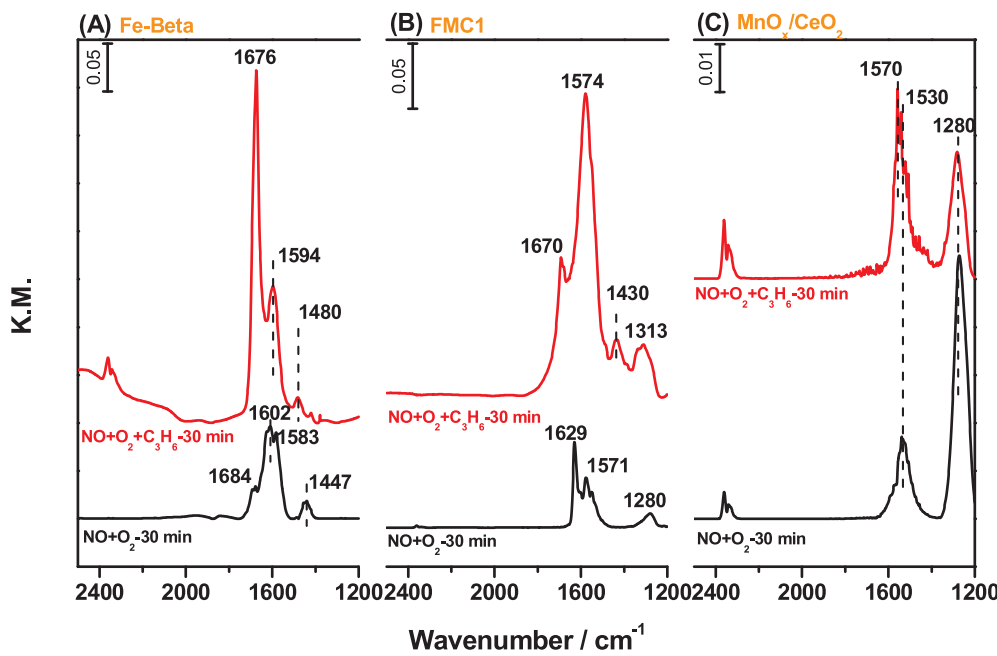


Fig. 7. IR spectra for Fe-Beta (A), FMC1 (B) and $\text{MnO}_x/\text{CeO}_2$ (C) after exposure to 500 ppm $\text{NO}/10\% \text{O}_2/\text{He}$ or 500 ppm $\text{NO}/10\% \text{O}_2/500 \text{ ppm C}_3\text{H}_6/\text{He}$ at 150 °C for 30 min.

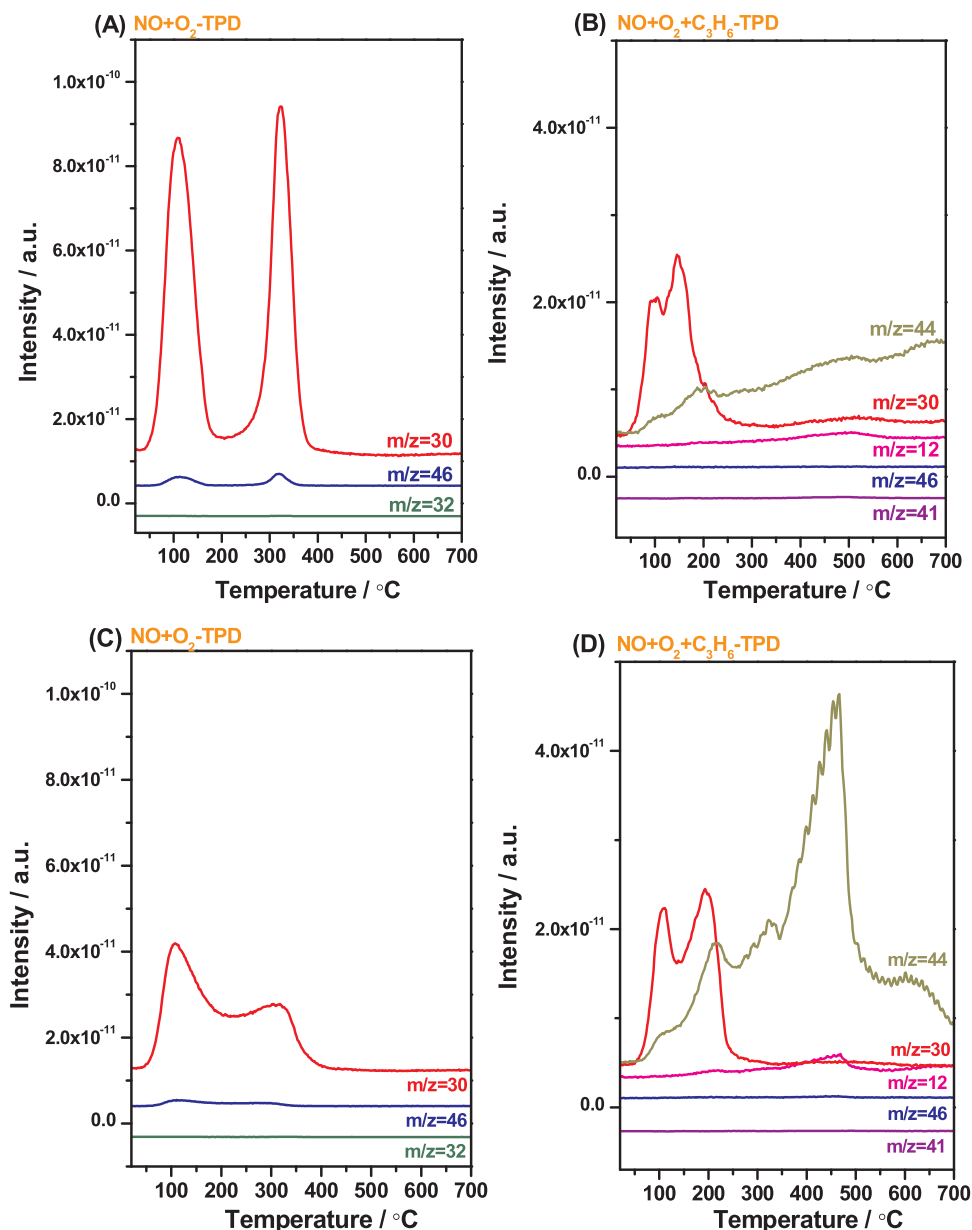


Fig. 8. MS data for Fe-Beta (A) and FMC1 (C) exposed to 500 ppm NO/10% O₂/Ar at RT followed by heating in a flow of Ar at 10 °C/min, and Fe-Beta (B) and FMC1 (D) exposed to 500 ppm NO/500 ppm C₃H₆/10% O₂/Ar at RT followed by heating in a flow of Ar at 10 °C/min.

Table 2
The amount of each species during TPD experiments.

Reaction process	Species	The amount of species (mmol/g _{cat})	
		Fe-Beta	FMC1
NO + O ₂ -Adsorption	NO	0.837	0.416
C ₃ H ₆ -Adsorption	C ₃ H ₆	2.242	0.961
NO + O ₂ + C ₃ H ₆ -Adsorption	NO	0.223	0.251
	C ₃ H ₆	0.782	0.387
NH ₃ -TPD	NH ₃	1.175	0.428

sites by the polymerized C₃H₆ species. On FMC1, bands at 1280, 1571 and 1629 cm⁻¹ are observed when NO + O₂ is introduced, as displayed in Fig. 7(B). The band at 1280 cm⁻¹ is attributed to $\nu(\text{NO}_3^-)$, while the bands at 1571 and 1629 cm⁻¹ are due to monodentate and bridged nitrates. When C₃H₆ is present, new bands assigned to $\nu_s(\text{COO})$ (1574 cm⁻¹) and $\nu(\text{C=O})$ (1670 cm⁻¹) have emerged, arising from

partial oxidation of C₃H₆ on the catalyst surface. Meanwhile, bands at 1430 and 1313 cm⁻¹ have developed, attributed to monodentate nitrates and bidentate nitrites [37–51].

Turning to the MnO_x/CeO₂ sample, bands at 1530 cm⁻¹ and 1280 cm⁻¹ are formed in the absence of C₃H₆ that can be assigned $\nu(\text{NO}_3^-)$ (see in Fig. 7(C)). When C₃H₆ is added to the feed gas, carboxyl species (1570 cm⁻¹) are formed, although the bands belonging to $\nu(\text{NO}_3^-)$ at 1530 and 1280 cm⁻¹ are still observed. From the foregoing results, it is clear that C₃H₆ is partially oxidized over the MnO_x/CeO₂ sample, whereas it polymerizes on Fe-Beta, blocking the sites for NO_x adsorption and becoming the dominant species on the surface.

Blocking of the NO_x adsorption sites on Fe-Beta by C₃H₆ is also evidenced by NO_x-TPD (Fig. 8) and the amount of each gaseous species desorbed being listed in Table 2. After saturation by the reactant gases, the samples are heated from room temperature to 700 °C in Ar. For Fe-Beta zeolite, NO (m/z = 30) has evolved as two peaks regardless of whether C₃H₆ is present during the adsorption step. Integration of the peaks shows that the amount of NO_x desorbed has decreased when C₃H₆

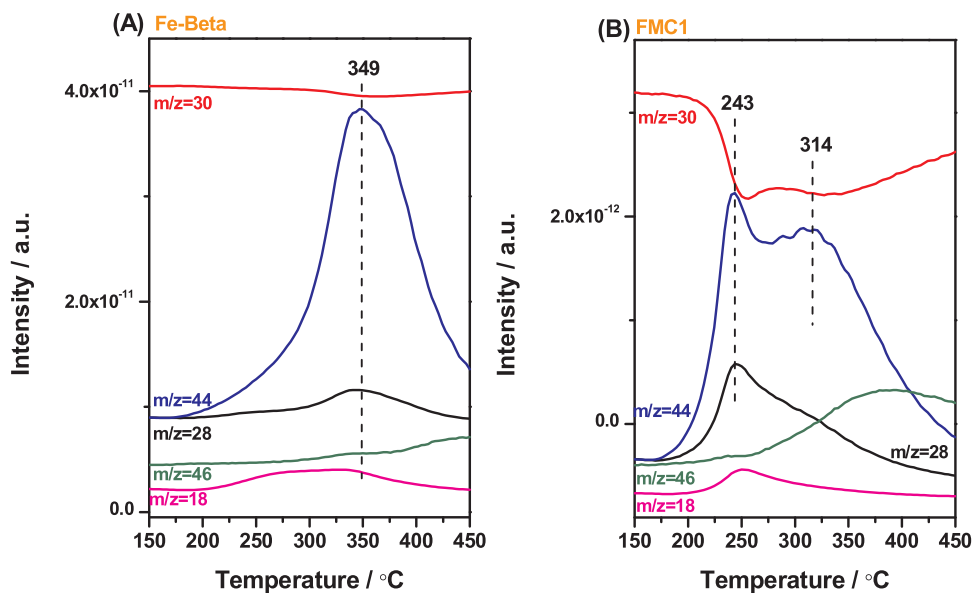


Fig. 9. MS signal obtained over (A) Fe-Beta and (B) FMC1 catalysts in 500 ppm NO/10% O₂/Ar after C₃H₆ adsorption using 500 ppm C₃H₆/Ar for 30 min; C₃H₆ adsorption was performed at 150 °C.

is present in the adsorption step, indicating that the adsorption of NO_x is inhibited by C₃H₆. Moreover, the NO_x desorbs at relatively low temperatures when C₃H₆ is present, suggesting that C₃H₆ blocks the strong adsorption sites for NO_x [52]. Moreover, minimal desorption of C₃H₆ is observed (Fig. S5), indicating that C₃H₆ is strongly bonded to the zeolite surface, this being in line with the DRIFTS data indicating that polymerization of C₃H₆ has occurred on Fe-Beta. For the hybrid catalyst, however, the presence of C₃H₆ during NO_x adsorption has less effect on the amount of NO_x subsequently desorbed during TPD than for Fe-Beta, albeit NO_x desorption above 300 °C is depressed to some degree. Additionally, gaseous CO₂ is generated at temperatures in excess of 400 °C, consistent with the higher oxidative capability of MnO_x/CeO₂ component in C₃H₆ oxidation.

3.5. Reaction between nitrogen oxides and propene adspecies

In order to evaluate whether or not the intermediates formed through C₃H₆ adsorption can be eliminated under SCR conditions, the catalyst samples are exposed to NO + O₂ after an initial saturation with C₃H₆, after which the temperature being raised from 150 °C to 450 °C. As indicated previously, C₃H₆ adsorption can result in the formation of various intermediates, C=O and COO species being present on FMC1, while polyene is mostly formed on the Fe-Beta surface (as shown in Fig. S6). As recorded in Fig. 9, during the temperature ramp, consumption peaks for NO can be clearly observed at 243 °C and 314 °C over FMC1, meanwhile the generation of CO₂ (m/z = 44) can be observed along with NO consumption. As to the peak at m/z = 28, it is reasonable to believe that it should belong to the production of N₂ due to the consumption of NO. From these results it can be concluded that upon increase of the temperature, C₃H₆-derived species can react with NO to produce N₂ and CO₂. In contrast, only trace amounts of NO consumption accompanied by a large CO₂ production peak can be detected over Fe-Beta catalyst at 349 °C, indicating that the polyene species on the Fe-Beta surface are apt to oxidize to CO₂ and H₂O rather than reacting with NO. The fact that NO consumption and N₂ production occur at lower temperatures on FMC1 than on Fe-Beta is consistent with the superior oxidation activity of the mixed oxide in FMC1, leading to the generation of reactive surface oxygenates.

3.6. Reaction between ammonia adspecies and nitrogen oxides

Combined DRIFTS and MS measurements have been employed to study the reaction between ammonia adspecies and nitrogen oxides. The catalysts are first exposed to NH₃/He at 150 °C for 30 min followed by He purging. Next, NO/O₂/C₃H₆/He is introduced, the results being shown in Fig. 10. Adsorbed NH₃ species have gave rise to bands at 1485 cm⁻¹ assigned to NH₄⁺ species, and at 1603 cm⁻¹, arising from NH₃ coordinated to the Fe-Beta and FMC1 surfaces. Upon introduction of NO + O₂ + C₃H₆, bands at 1594 and 1695 cm⁻¹ have appeared in the case of Fe-Beta, together with a shoulder at 1668 and a band at 2926 cm⁻¹. These bands can be assigned to ν (C=C) in polyene species, ν (C=O), adsorbed NO₂ and ν (CH₃), respectively. Notably, the band belonging to NH₃ adsorbed on Brønsted acid sites (1485 cm⁻¹) has initially decreased due to the reaction of NH₄⁺ with adsorbed NO_x, as evidenced by the production of N₂ (m/z = 28) as shown in Fig. 10. However, the band intensity has reached a fairly constant value quickly, which may be the result of C₃H₆ inhibition on NO_x adsorption. In contrast, over the FMC1 catalyst, the introduction of NO + O₂ + C₃H₆ has caused the disappearance of adsorbed NH₃ species (1474, 1617 cm⁻¹), while several new bands at 1678, 1572, 1432 and 1334 cm⁻¹ have increased in intensity with time. These bands can be assigned to ν (C=O), ν _s(COO), ν _{as}(COO) and bidentate nitrites, respectively. Comparing the gas phase products detected by MS, much larger amount of N₂, H₂O and CO₂ are generated over FMC1, this being in line with its superior NH₃-SCR activity compared to Fe-Beta when C₃H₆ is present. It is also worth noting that over the FMC1 sample, two events are observed which may give rise to a peak at m/z = 28. The first event is assigned to the generation of N₂ on the FMC1 surface during switching of the feed gas, while the other is associated with the formation of CO_x from C₃H₆ oxidation which gives rise to signals at 44 and 28 (due to CO₂ fragmentation in the MS).

3.7. Stability of intermediates

After exposure of the NH₃-loaded samples to NO + O₂ + C₃H₆, the catalysts are heated from 150 °C to the desired temperature in Ar in order to study the stability of the intermediates present. As shown in Fig. 11, it can be inferred that mainly polyene and C=O species have been present on the Fe-Beta surface, the intensity of these bands showing little change as the temperature has raised from 150 °C to

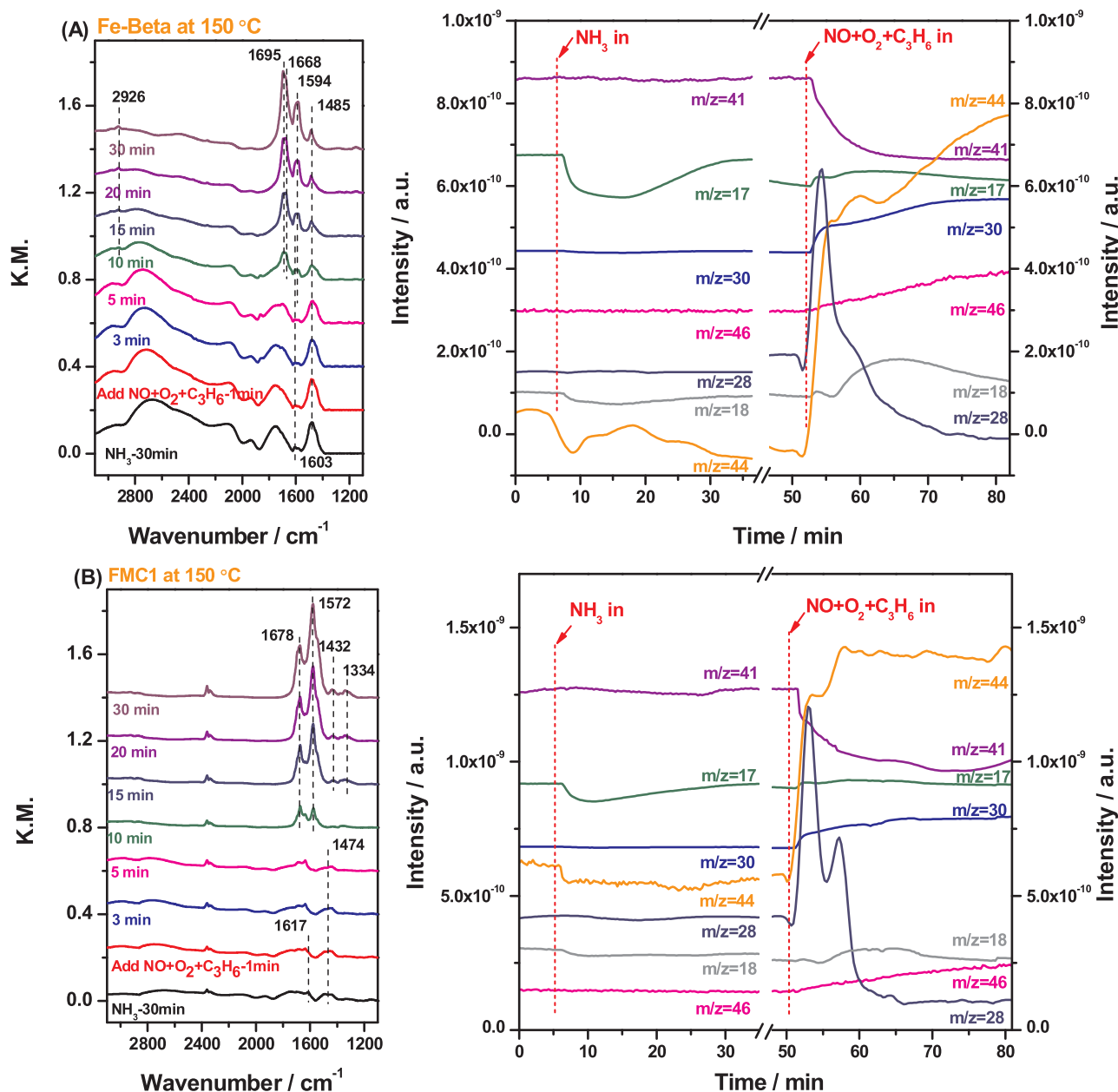


Fig. 10. IR spectra (left panel) and MS data (right panel) for (A) Fe-Beta and (B) FMC1 pretreated by exposure to 500 ppm NH_3/Ar followed by exposure to 500 ppm $\text{C}_3\text{H}_6/500 \text{ ppm NO}/10\% \text{ O}_2/\text{Ar}$ at 150 °C for various times.

200 °C. With further increase of the temperature, the band belonging to $\nu(\text{C}=\text{O})$ decreases in intensity while gaseous CO is detected by MS (depicted in Fig. S7). The band belonging to adsorbed NO_2 at 1668 cm^{-1} also diminishes and at the same time a band at 1880 cm^{-1} assigned to gaseous NO arises indicative of nitrite decomposition. However, changes in the MS signal at $m/z = 30$ are hard to detect, presumably due to the low NO concentration (shown in Fig. S7). Notably, the bands at 1594 cm^{-1} and 2923 cm^{-1} assigned to $\nu(\text{C}=\text{C})$ in polyene and $\nu(\text{CH}_3)$, respectively, are barely changed. From this it can be inferred that upon adsorption on Fe-Beta, C_3H_6 transforms to polymerized species, even at low temperature (150 °C). Indeed, these species are difficult to eliminate below 300 °C, and can therefore inhibit SCR activity. For FMC1, the $\nu(\text{C}=\text{O})$ band (1678 cm^{-1}) has decreased in intensity with increase of the temperature, while the $\nu(\text{COO})$ band (1432 cm^{-1}) has increased in intensity up to 250 °C and then decreased above 300 °C. This phenomenon can be explained on the basis that the $\text{C}=\text{O}$ species first convert to COO species, the latter undergoing further

oxidation to gaseous CO_2 upon increase of the temperature. This is substantiated by MS data shown in the inset of Fig. 11, CO_2 being evolved in two main steps at 250 °C–350 °C.

4. Discussion

According to the literature, unburned hydrocarbons (HCs) in diesel engine exhaust of which propene (kinetic diameter of 4.5 Å) is a typical constituent - can deactivate zeolites such as ZSM-5 and BEA (possessing pore diameters of approximately of 5.5 Å and 6.5 Å, respectively [10,16]). It is generally accepted that the carbonaceous deposits formed from adsorbed HCs can block the active sites of the catalyst [11,17], although little is known about the exact composition of these deposits. Previous results demonstrate that coke formation is mainly related to the pore structure and acidity of the zeolite [17]. Zeolites with larger pore size ($> 4.5 \text{ \AA}$) and strong acidity are more susceptible to deactivation by C_3H_6 . The degradation of catalyst activity can also be ascribed

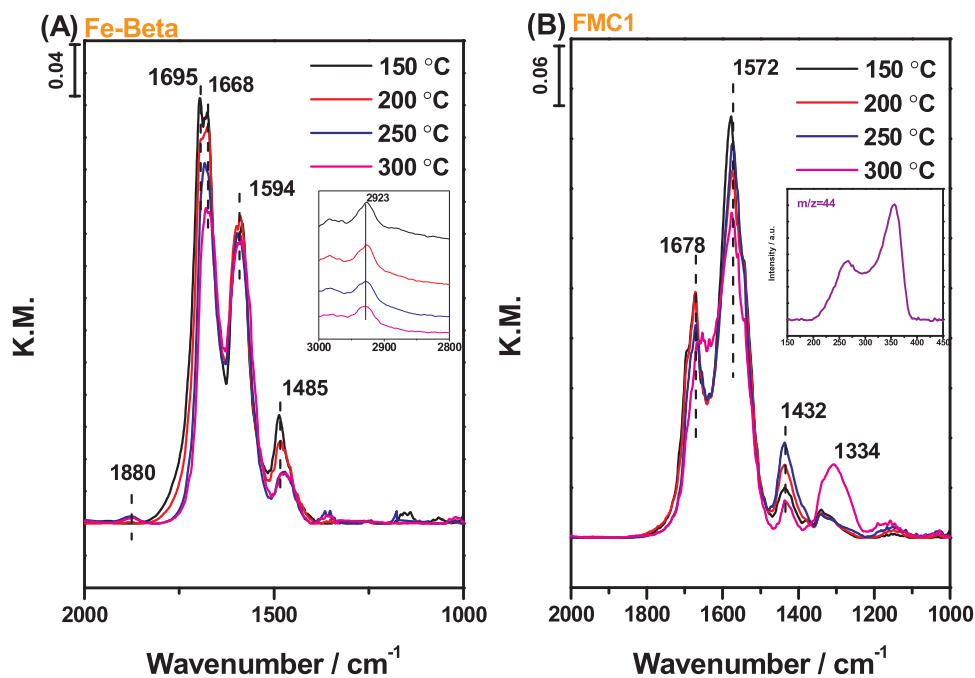


Fig. 11. IR spectra showing consumption of intermediates over (A) Fe-Beta and (B) FMC1 in flowing Ar at different temperatures after exposure to 500 ppm NH₃/500 ppm NO/10% O₂/ 500 ppm C₃H₆/Ar at 150 °C.

to the competitive adsorption of C₃H₆ with NH₃ and/or NO on the catalyst surface, whereby the formation of intermediates during the NH₃-SCR reaction is inhibited [10]. In order to alleviate the effect of C₃H₆, Ma et al. [10] have designed a Fe-BEA monolith catalyst coating modified with MOR to restrict the diffusion of C₃H₆ in BEA cavities and reduce the surface acidity, thereby improving the tolerance of the catalyst towards HC_s. Zhang et al. [3] have synthesized a core-shell structured meso-SSZ-13 material by combining controlled desilication with subsequent self-assembly, resulting in a material with smaller pores than the kinetic diameter of propene, thereby inhibiting direct access of propene to the zeolite channels. These workers have also found that due to the coverage of the external surface by the shell, the amount of exposed sites for propene oxidation is decreased, effectively reducing propene polymerization. The use of additives is another effective method to improve the hydrocarbon resistance of HBBA - based catalysts. Feng et al. [14] have used incipient wetness impregnation to prepare CuFe/Ce/Beta. By adding Ce, the presence of strong acid sites is suppressed, which acting as the main adsorption sites for propene. Shi et al. [17] have used CeO₂ as an additive to minimize the poisoning effects of propene on HBBA. The external surface of HBBA is coated by CeO₂ forming a core-shell structure, and it is shown that the improved resistance to propene poisoning is due to a combination of (i) decreased C₃H₆ adsorption and (ii) C₃H₆ oxidation by the ceria. Overall, while some progress has been made towards improving the hydrocarbon resistance of zeolite catalysts, the exact nature of the species acting as poisons is unclear, while considerable scope exists to improve catalyst activity further.

In the present work, we have designed and synthesized hybrid catalysts exemplified by FMC1. During calcination, a chemical interaction arose between the mechanically mixed Fe-Beta and MnO_x/CeO₂. Specifically, a new phase corresponding to (Mn_{0.983}Fe_{0.017})₂O₃ was formed, while the redox properties of the hybrid catalyst were modified as evidenced by H₂-TPR (Fig. 2). FMC1 catalyst, being enriched with Mn³⁺, exhibits relatively fewer active oxygen species that are reduced at low temperature (302 °C in H₂-TPR). Comparatively, the MnO_x/CeO₂ sample, which is characterized by a higher concentration of Mn⁴⁺ and active oxygen species, has better catalytic activity in both C₃H₆ oxidation (Fig. 5(B)) and NH₃ oxidation, although the latter reaction leads

to relatively lower high temperature NO_x conversion and increased N₂O generation. The hybrid FMC catalysts exhibit excellent SCR activity across the whole temperature window and the ratio of the zeolite to oxide can be tuned according to the requirements of the application (as shown in Fig. 1): higher fractions of the oxide component provide better low temperature activity but higher N₂O yield and lower NO_x conversion at high temperature. The results imply that the higher oxidation activity associated with higher fractions of the oxide component leads to better low temperature NH₃-SCR activity, indicating that NO oxidation to NO₂ represents the rate limiting step for the low-temperature SCR reaction. Higher amounts of Mn⁴⁺ favor NO oxidation, and therefore facilitate the low-temperature SCR reaction.

In order to ascertain the function of MnO_x/CeO₂ in the hybrid catalyst, mechanistic studies have been conducted. We have observed that the improvement in activity achieved by catalyst FMC1 is not due to direct participation in C₃H₆-SCR or C₃H₆ combustion by MnO_x/CeO₂.

As C₃H₆ is present in the feed gas, C₃H₆ polymerization has readily occurred on the Fe-Beta surface due to its abundant acid sites, blocking the sites for NO adsorption and further reaction. After combining the oxidation components with Fe-Beta, the partial oxidation of C₃H₆ to oxygenates occurs more readily than polymerization as shown in Fig. 6, and thus the catalyst surface is not subject to fouling. Besides that, due to the higher oxidation activity of MnO_x/CeO₂ compared to Fe-Beta, the hybrid catalyst can generate more intermediates containing C=O and COO functionalities during C₃H₆ adsorption than on Fe-Beta, and these oxygenate species are able to react with NO_x on FMC1 to enhance the overall activity. Such improvement in activity is further evidenced by the results of combined DRIFTS and MS experiments shown in Fig. 10. However, polyene species generated on Fe-Beta surface hardly react with NO, but are directly oxidized to CO₂ and H₂O at elevated temperatures (349 °C, Fig. 9). Since the surface polymer species are difficult to eliminate at temperatures below 300 °C (shown in Fig. 11), the SCR activity is severely inhibited. Based on the foregoing, it is clear that mixing Fe-Beta zeolite with MnO_x/CeO₂ oxide enhanced the oxidation ability of the catalysts. Thus, the much higher oxidative capability of FMC1 can not only partially oxidize C₃H₆ into oxygenates, but also enables the reaction of C₃H₆ - derived species with NO at low temperatures, thereby mitigating the effects of C₃H₆ on the NH₃-SCR of NO_x.

over Fe-Beta catalysts.

5. Conclusions

The presence of C_3H_6 during NH_3 -SCR is known to depress the activity of zeolite catalysts with medium to large pores such as metal ion exchanged Beta and ZSM-5 due to fouling and pore blocking. Herein, we propose a simple and effective protocol to mitigate this poisoning effect by mechanically mixing the zeolite with an oxidation catalyst. The resulting FMC1 sample exhibits excellent SCR activity in the presence of C_3H_6 across the whole temperature window. MnO_x/CeO_2 in the hybrid catalysts plays several important roles: 1) converting C_3H_6 into oxygenated intermediates, thereby avoiding polymerization reactions on the zeolite surface and associated pore blocking; 2) reducing the competitive adsorption between NO_x and C_3H_6 to facilitate the NH_3 -SCR reaction; 3) catalyzing the reaction of oxygenates and NO_x at low temperatures to improve the overall NO_x conversion activity.

Acknowledgement

Thanks Doctor U. Mueller from BASF for providing the BEA zeolite support. The work was supported by the National Key R&D Program of China (No. 2017YFA0700103), and National Natural Science Foundation of China (Nos. 21577013 and 21707015).

Appendix A. Supplementary data

Supplementary material related to this article can be found, in the online version, at doi:<https://doi.org/10.1016/j.apcatb.2018.09.072>.

References

- [1] Y. Zhu, B. Chen, R. Zhao, Q. Zhao, H. Gies, F. Xiao, D. Vos, T. Yokoi, X. Bao, U. Kolb, M. Feyen, S. Maurer, A. Moini, U. Müller, C. Shi, W. Zhang, *Catal. Sci. Technol.* 6 (2016) 6581–6592.
- [2] S. Brandenberger, O. Kröcher, A. Tissler, R. Althoff, *Appl. Catal. B* 95 (2010) 348–357.
- [3] T. Zhang, F. Qiu, J. Li, *Appl. Catal. B* 195 (2016) 48–58.
- [4] R. Nedyalkova, S. Shwan, M. Skoglundh, L. Olsson, *Appl. Catal. B* 138–139 (2013) 373–380.
- [5] L. Xu, C. Shi, B. Chen, Q. Zhao, Y. Zhu, H. Gies, F. Xiao, D. De Vos, T. Yokoi, X. Bao, U. Kolb, M. Feyen, S. Maurer, A. Moini, U. Müller, W. Zhang, *Microporous Mesoporous Mater.* 236 (2016) 211–217.
- [6] P. Balle, B. Geiger, D. Klukowski, M. Pignatelli, S. Wohnrau, M. Menzel, I. Zirkwa, G. Brunklaus, S. Kureti, *Appl. Catal. B* 91 (2009) 587–595.
- [7] L. Xu, C. Shi, Z. Zhang, H. Gies, F. Xiao, D. Vos, T. Yokoi, X. Bao, M. Feyen, S. Maurer, B. Yilmaz, U. Müller, W. Zhang, *Microporous Mesoporous Mater.* 200 (2014) 304–310.
- [8] P. Sazama, B. Wichterlová, Š. Sklenák, V. Parvulescu, N. Candu, G. Sádovská, J. Dědeček, P. Klein, V. Pashkova, P. Šťastný, *J. Catal.* 318 (2014) 22–33.
- [9] R. Zhang, N. Liu, Z. Lei, B. Chen, *Chem. Rev.* 116 (2016) 3658–3721.
- [10] L. Ma, J. Li, Y. Cheng, C. Lambert, L. Fu, *Environ. Sci. Technol.* 46 (2012) 1747–1754.
- [11] L. Ma, W. Su, Z. Li, J. Li, L. Fu, J. Hao, *Catal. Today* 245 (2015) 16–21.
- [12] C. He, Y. Wang, Y. Cheng, C. Lambert, R. Yang, *Appl. Catal. A Gen.* 368 (2009) 121–126.
- [13] I. Malpartida, O. Marie, P. Bazin, M. Daturi, X. Jeandel, *Appl. Catal. B* 102 (2011) 190–200.
- [14] X. Feng, Y. Cao, L. Lan, C. Lin, Y. Li, H. Xu, M. Gong, Y. Chen, *Chem. Eng. J.* 302 (2016) 697–706.
- [15] I. Heo, Y. Lee, I. Nam, J. Choung, J. Lee, H. Kim, *Microporous Mesoporous Mater.* 141 (2011) 8–15.
- [16] J. Li, R. Zhu, Y. Cheng, C. Lambert, R. Yang, *Environ. Sci. Technol.* 44 (2010) 1799–1805.
- [17] Y. Shi, X. Wang, Y. Xia, C. Sun, C. Zhao, S. Li, W. Li, *Mol. Catal.* 433 (2017) 265–273.
- [18] J. Luo, A. Yezers, C. Henry, H. Hess, K. Kamasamudram, H. Chen, W. Epling, *Hydrocarbon Poisoning of Cu-Zeolite SCR Catalysts*, SAE International, 2012.
- [19] C. Liu, J. Shi, C. Gao, C. Niu, *Appl. Catal. A Gen.* 522 (2016) 54–69.
- [20] D. Delimaris, T. Ioannides, *Appl. Catal. B* 84 (2008) 303–312.
- [21] X. Tang, Y. Li, X. Huang, Y. Xu, H. Zhu, J. Wang, W. Shen, *Appl. Catal. B* 62 (2006) 265–273.
- [22] S. Jiang, R. Zhou, *Fuel Process. Technol.* 133 (2015) 220–226.
- [23] R. Jin, Y. Liu, Y. Wang, W. Cen, Z. Wu, H. Wang, X. Weng, *Appl. Catal. B* 148–149 (2014) 582–588.
- [24] L. France, Q. Yang, W. Li, Z. Chen, J. Guang, D. Guo, L. Wang, X. Li, *Appl. Catal. B* 206 (2017) 203–215.
- [25] B. Xie, J. Song, L. Ren, Y. Ji, J. Li, F. Xiao, *Chem. Mater.* 20 (2008) 4533–4535.
- [26] B. Chen, C. Shi, M. Crocker, Y. Wang, A. Zhu, *Appl. Catal. B* 132–133 (2013) 245–255.
- [27] M. Salazar, R. Becker, W. Grünert, *Appl. Catal. B* 165 (2015) 316–327.
- [28] H. Chen, A. Sayari, A. Adnot, F. Larachi, *Appl. Catal. B* 32 (2001) 195–204.
- [29] S. Deng, H. Liu, W. Zhou, J. Huang, G. Yu, J. Hazard. Mater. 186 (2011) 1360–1366.
- [30] T. Rao, M. Shen, L. Jia, J. Hao, J. Wang, *Catal. Commun.* 8 (2007) 1743–1747.
- [31] Z. Liu, Y. Yi, S. Zhang, T. Zhu, J. Zhu, J. Wang, *Catal. Today* 216 (2013) 76–81.
- [32] B. Tan, K. Klabunde, P. Sherwood, *J. Am. Chem. Soc.* 113 (1991) 855–861.
- [33] G. Qi, R. Yang, *J. Phys. Chem. B* 108 (2004) 15738–15747.
- [34] Z. Zhang, B. Chen, X. Wang, L. Xu, C. Au, C. Shi, M. Crocker, *Appl. Catal. B* 165 (2015) 232–244.
- [35] G. Qi, R. Yang, R. Chang, *Appl. Catal. B* 51 (2004) 93–106.
- [36] Z. Wu, R. Jin, H. Wang, Y. Liu, *Catal. Commun.* 10 (2009) 935–939.
- [37] P. Kumar, M. Reddy, B. Hyun-Sook, H. Phil, *Catal. Letters* 131 (2009) 85–97.
- [38] F. Dorado, P. García, A. Lucas, M. Ramos, A. Romero, *J. Mol. Catal. A Chem.* 332 (2010) 45–52.
- [39] V. Matyshak, O. Krylov, *Catal. Today* 25 (1995) 1–87.
- [40] R. Long, R. Yang, *J. Phys. Chem. B* 103 (1999) 2232–2238.
- [41] N. Hayes, R. Joyner, E. Shiro, *Appl. Catal. B* 8 (1996) 343–363.
- [42] S. Park, Y. Park, S. Park, L. Kevan, *J. Chem. Soc. Faraday Trans. 2* (2000) 5500–5509.
- [43] I. Cayırcıtepe, A. Naydenov, G. Ivanov, M. Kantcheva, *Catal. Letters* 132 (2009) 438–449.
- [44] L. Li, N. Guan, *Microporous Mesoporous Mater.* 117 (2009) 450–457.
- [45] J. Liu, X. Li, Q. Zhao, C. Hao, D. Zhang, *Environ. Sci. Technol.* 47 (2013) 4528–4535.
- [46] K. Góra-Marek, K. Brylewská, K. Tarach, M. Rutkowska, M. Jabłońska, M. Choi, L. Chmielarz, *Appl. Catal. B* 179 (2015) 589–598.
- [47] R. Long, R. Yang, *J. Catal.* 207 (2002) 274–285.
- [48] G. Qi, *J. Catal.* 226 (2004) 120–128.
- [49] L. Xu, X. Li, M. Crocker, Z. Zhang, A. Zhu, C. Shi, *J. Mol. Catal. A Chem.* 378 (2013) 82–90.
- [50] F. Prinetto, G. Ghiootti, I. Nova, L. Lietti, E. Tronconi, P. Forzatti, *J. Phys. Chem. B* 105 (2001) 12732–12745.
- [51] Z. Zhang, L. Chen, Z. Li, P. Li, F. Yuan, X. Niu, Y. Zhu, *Catal. Sci. Technol.* 6 (2016) 7151–7162.
- [52] M. Iwasaki, K. Yamazaki, K. Banno, H. Shinjoh, *J. Catal.* 260 (2008) 205–216.